

OpenICS: Open Image Compressive Sensing Toolbox and Benchmark

Jonathan Zhao¹, Matthew Westerham¹, Mark Lakatos-Toth¹, Zhikang Zhang¹, Avi Moskoff², Fengbo Ren

Parallel Systems and Computing Laboratory

Arizona State University

Tempe, USA

jjzhao@asu.edu, mkweste1@asu.edu, mlakato1@asu.edu, zzhan362@asu.edu, amoskoff@asu.edu, renfengbo@asu.edu

Abstract—We present OpenICS, an image compressive sensing toolbox that includes multiple image compressive sensing and reconstruction algorithms proposed in the past decade. Due to the lack of standardization in the implementation and evaluation of the proposed algorithms, the application of image compressive sensing in the real-world is limited. We believe this toolbox is the first framework that provides a unified and standardized implementation of multiple image compressive sensing algorithms. In addition, we also conduct a benchmarking study on the methods included in this framework from two aspects: reconstruction accuracy and reconstruction efficiency. We wish this toolbox and benchmark can serve the growing research community of compressive sensing and the industry applying image compressive sensing to new problems as well as developing new methods more efficiently. Code and models are available at <https://github.com/PSCLab-ASU/OpenICS>. The project is still under maintenance, and we will keep this document updated.

Index Terms—compressive sensing, computer vision, machine learning, signal processing

I. INTRODUCTION

Compressive sensing is a signal sensing technique that performs the sensing and compression of signals simultaneously to reduce the sensing cost without losing information. Over the past decade, there is a wide variety of image compressive sensing reconstruction methods proposed. However, due to the lack of standardization in the implementation and evaluation of the proposed algorithms, the application of image compressive sensing in the real-world is still limited. Towards the goal of efficient deployment and evaluation of image compressive sensing, we build OpenICS which is an image compressive sensing toolbox containing multiple image compressive sensing reconstruction methods implemented in a unified interface and structure.

Major features of OpenICS are 1. **Unified interface**. We rewrite the code of multiple image compressive sensing algorithms to build a unified interface for all the methods. This unified design greatly improves the usability and availability of our toolbox. 2. **Modular design**. Each method locates in a separate folder, and there is no cross-dependency between different methods. This modular design improves the reusability of our toolbox. 3. **Out-of-the-box usage**. Our toolbox contains the most representative methods of image compressive sensing methods. See Section 2 for the full list.

In addition to the toolbox we implemented, we also propose a benchmark to evaluate all the methods included in the toolbox from two aspects: reconstruction accuracy and reconstruction speed. The benchmark results include the performance of all the methods evaluated on six different datasets and five different compression ratios. We believe our benchmark is the most complete benchmark in the domain of image compressive sensing so far in terms of the variety of datasets and the range of compression ratios.

Our contribution are summarized as follows:

1. We provide a toolbox in the domain of image compressive sensing that consists of multiple most representative algorithms in this domain. The toolbox has a unified interface, modular design, and it can be used out of box.

2. We propose a benchmark in the domain of image compressive sensing and use it to evaluate the methods included in our toolbox. It is by far the most complete benchmark in the domain of image compressive sensing in terms of the variety of datasets and the range of compression ratios.

II. METHODS INCLUDED

OpenICS contains implementations of multiple image CS reconstruction methods. Based on whether the method is data-dependent, we divide implemented methods into two categories: Model-based methods and data-driven methods.

A. Model-based Methods

Model-based methods use pre-defined models based on prior knowledge of the signals to perform the reconstruction. The included model-based methods are listed and summarized in table I.

L1 [1]: The first reconstruction methods in the domain of compressive sensing(Only the total-variation-based methods are currently implemented).

NLR-CS [2]: A reconstruction method based on non-local low-rank regularization.

TVAL-3 [3]: An efficient image reconstruction method based on total variation minimization.

D-AMP [4]: An reconstruction method based on model-based image denoising algorithms.

Methods	Data dependent	Running process	Platform
L1	No	Iterative	CPU
TVAL-3	No	Iterative	CPU
NLR-CS	No	Iterative	CPU
D-AMP	No	Iterative	CPU
ReconNet	Yes	End-to-end	GPU
ISTA-Net	Yes	End-to-end	GPU
LDAMP	Yes	End-to-end	GPU
CSGM	Yes	Iterative	GPU
LAPRAN	Yes	End-to-end	GPU
CSGAN	Yes	Iterative	GPU

TABLE I
LIST OF METHODS INCLUDED IN OPENICS

B. Data-driven Methods

Data-driven methods do not rely on pre-defined models of signals. Instead, they use neural networks to model the images and perform the reconstruction tasks. The included data-driven methods are listed below.

ReconNet [5]: An end-to-end reconstruction network based on convolutional neural networks.

LDAMP [6]: An end-to-end reconstruction network built from the unrolled iterative image denoising process by replacing the model-based image denoisers with neural-network-based denoisers.

ISTA-Net [7]: An end-to-end reconstruction network built by unrolling the conventional iterative shrinkage-thresholding algorithm.

LAPRAN [8]: An end-to-end reconstruction network based on deep laplacian pyramid neural networks.

CSGM [9]: An iterative reconstruction method based on generative adversial neural network.

CSGAN [10]: A variant of CSGM method enhanced by meta-learning to improve reconstruction speed.

III. ARCHITECTURE

A. Toolbox Structure

There are two programing languages used to implement all the methods. L1, NLR-CS, TVAL-3, D-AMP are implemented in Matlab. ReconNet, ISTA-Net, LAPRAN are implemented in Python with Pytorch [11]. CSGM, CSGAN, LDAMP are implemented in Python with Tensorflow [12].

We provide a unified interface to run all the methods. Specifically, the common parameters of all methods are listed as follows:

- 1) dataset: the name of dataset to be used
- 2) input_channel: number of channels training/testing images have
- 3) input_width: width of training/testing images
- 4) input_height: height of training/testing images
- 5) m: number of measurements/outputs of sensing matrix
- 6) n: number of inputs to sensing matrix

Besides, there are method-specific parameters that are included in a container-like object called "specifics". In python, it is a dictionary with its keys as parameter names and its values as actual parameters. In Matlab, it is a structure array with its

field names as parameter names, and its field values are the parameters.

We also provide the functionality to directly call certain methods from the main interface. The parameters of the main interface are listed below:

- 1) sensing: method of sensing
- 2) reconstruction: method of reconstruction
- 3) stage: training or testing(model-based methods do not have this parameter)
- 4) default: will use default parameters if it's true. Will override other parameters set manually.
- 5) dataset: same as method's corresponding parameter.
- 6) input_channel: same as method's corresponding parameter.
- 7) input_width: same as method's corresponding parameter.
- 8) input_height: same as method's corresponding parameter.
- 9) m: same as method's corresponding parameter.
- 10) n: same as method's corresponding parameter.
- 11) specifics: specific parameter settings of chosen reconstruction method. Will be passed to the actual method.

Given an image to be sensed and reconstructed, for model-based methods, it can be directly reconstructed by calling the main function of specific methods. For data-driven methods, the networks of specific methods have to be trained first. We provide pre-trained networks of each method at five compression ratios(2,4,8,16,32) on six datasets. We also provide the functionality of training new networks on new datasets and compression ratios from scratch.

More details regarding how to use our code are listed in the main page of our Github repository(<https://github.com/PSCLab-ASU/OpenICS>).

IV. BENCHMARKS

A. Benchmark Design

Dataset. We use six widely used datasets to evaluate all the methods in benchmark. They are MNIST [13], CIFAR10 [14], CIFAR10(grayscale), CELEBA [15], Bigset, Bigset(grayscale). Bigset stands for a manually composed dataset. It was initially used in [16]–[18] in the domain of single image super-resolution. Later it was used in LAPRAN [8] for image compressive sensing. The training set of Bigset was composed of 91 images from [19] and 200 images from the BSD [20] dataset. The 291 images are augmented (rotation and flip) and cut into 228688 patches as training samples. The testing set of Bigset consists of image patches from Set5 [21] and Set14 [22] with same patch size. For MNIST, CIFAR10, CIFAR10(gray), the image size of samples is 32x32. For CELEBA, Bigset(gray) and Bigset, the image size of samples is 64x64.

Compression ratios. We take five different compression ratios to evaluate each method: 2,4,8,16,32. The compression is always performed channel-wise, i.e., for colored images(with RGB color channels), we perform the compression over each channel separately. The measurements of all three channels

are then grouped together for subsequent reconstruction. The training procedure of each data-driven method is almost the same as the original training guideline provided by the original authors. The discrepancy is detailed in our github repository.

Metrics. We evaluate all the methods from two aspects: reconstruction accuracy and reconstruction speed. The reconstruction accuracy is quantified with two metrics: PSNR(0-48) and SSIM(0-1) between reconstructed images and original images in the testing set. Higher values indicate higher accuracy. For each experiment we conduct, the reported results are the averaged values of both metrics over all the samples of the corresponding testing set. The reconstruction speed is quantified with the number of images reconstructed per second. This value is averaged over all the samples in the testing set as well.

Benchmark calculation. After obtaining the all raw benchmark results of each method (total of 6 datasets \times 5 compression ratios \times 3 metrics = 90 raw results), we use the following equation to calculate the final benchmark score:

$$score = \sum_{i=1}^{90} w_{dataset} * w_{cr} * w_{metric} * \bar{v}_i \quad (1)$$

\bar{v}_i is the i th normalized raw experiment result. Due to the different value ranges of each metric, we have to normalize the raw values to 0-100 range to avoid the dominance of one metric over the others. The function used to normalize PSNR values is $\bar{v} = 10^{\frac{v}{48}-1} * 100$. The function used to normalize SSIM values is $\bar{v} = 10^{v-1} * 100$. The function used to normalize reconstruction speed values is $\bar{v} = \frac{100}{1+1/\log(1+v)}$. $w_{dataset}$ is the weight of the corresponding dataset of v_i . Different weights are assigned to different datasets according to their relative complexity in reconstruction compared with other datasets. The relative complexity is determined based on the results reported in literatures [1]–[10] in the domain of image compressive sensing.

w_{cr} is the weight of the corresponding compression ratio of v_i . Since images compressed at higher compression ratios are more difficult to reconstruct than images compressed at lower compression ratios, we assign higher weights to higher compression ratios.

w_{metric} is the weight of corresponding metric of v_i . we assign different weights to different metrics as PSNR : SSIM : Speed = 1 : 1 : 2. As such, there is no bias between reconstruction accuracy and reconstruction speed. One can specify own weights to different metrics to make the score reflects one's own preferences.

The actual weights are listed in table II, table III and table IV.

B. Benchmark Results

The raw benchmark results are listed in Table VI, VII, VIII, IX, X, XI, XII, XIII, XIV and XV in the appendix. The benchmark score of each method is shown in Table V and Fig 1.

LAPRAN has the highest benchmark score due to its prominent performance in accuracy and speed. LDAMP has

Dataset	Weight
MNIST	1/21
CelebA	4/21
CIFAR10	3/21
CIFAR10 Gray	2/21
Bigset	6/21
Bigset Gray	5/21

TABLE II
WEIGHTS OF DATASETS

Compression ratio	Weight
2	1/31
4	2/31
8	4/31
16	8/31
32	16/31

TABLE III
WEIGHTS OF COMPRESSION RATIOS

Metric	Weight
PSNR	1/4
SSIM	1/4
Reconstruction speed	1/2

TABLE IV
WEIGHTS OF METRICS

Method	Accuracy	Speed	Score
LDAMP	24.24	19.21	43.46
ISTA-Net	20.40	30.02	50.42
CSGAN	19.03	22.29	41.32
LAPRAN	23.60	32.69	56.30
CSGM	13.27	0.11	13.38
ReconNet	18.78	35.28	54.06
TVAL-3	18.92	18.43	37.35
L1	19.69	3.78	23.46
D-AMP	21.83	2.35	24.19
NLR-CS	20.35	1.69	22.04

TABLE V
THE BENCHMARK SCORES

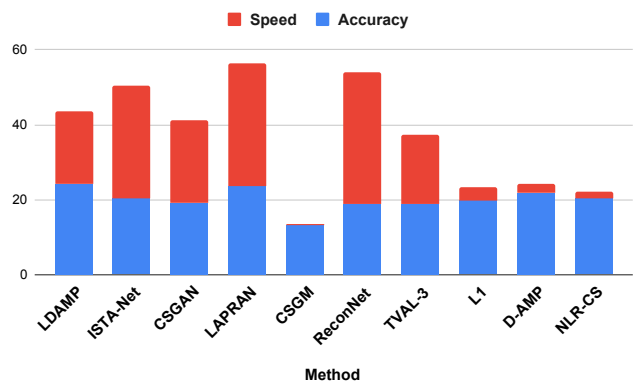


Fig. 1. The benchmark scores

the highest performance in accuracy but bad performance in speed due to its heavyweight design of network structure (more than 200 neural layers). ReconNet has the highest performance in reconstruction speed due to its lightweight design in structure (only seven layers), but its performance in accuracy is limited as well. In general, model-based methods have lower performance on both accuracy and speed than data-driven methods due to their static, pre-defined signal prior and iterative running process. CSGM is a special case in data-driven methods. The unsatisfying performance in accuracy is due to the GAN model it uses, which is DCGAN [23] proposed in 2015. Over the past few years, there have been more successful GAN models proposed, such as StyleGAN [24] that has much higher performance in modeling signals from data, which may improve the performance of CSGM if it is used. For all the model-based methods, NLR-CS and D-AMP have higher performance in reconstruction accuracy but lower performance in reconstruction speed compared with the other two methods.

To conclude, in general, data-driven methods achieve the highest performance in terms of accuracy and performance. With enough training data and hardware platforms that have sufficient computation capacity, one should always choose end-to-end data-driven methods. If there is no sufficient data, one should choose model-based methods that have the highest reconstruction accuracy. If the reconstruction speed is a critical factor to consider as well, TVAL-3 has a significantly higher reconstruction speed than other model-based methods and comparable reconstruction accuracy to other methods.

ACKNOWLEDGMENT

This work is supported by the Research Experiences for Undergraduates (REU) funding of an NSF grant (IIS/CPS-1652038) and the Fulton Undergraduate Research Initiative (FURI) program at Arizona State University. Part of the NVIDIA GPUs used for this work was donated by NVIDIA Corporation. The CPU servers used for this work were donated by Intel Corporation.

REFERENCES

- [1] E. Candes and J. Romberg, “l1-magic: Recovery of sparse signals via convex programming,” URL: www.acm.caltech.edu/l1magic/downloads/l1magic.pdf, vol. 4, p. 14, 2005.
- [2] W. Dong, G. Shi, X. Li, Y. Ma, and F. Huang, “Compressive sensing via nonlocal low-rank regularization,” *IEEE transactions on image processing*, vol. 23, no. 8, pp. 3618–3632, 2014.
- [3] C. Li, W. Yin, H. Jiang, and Y. Zhang, “An efficient augmented lagrangian method with applications to total variation minimization,” *Computational Optimization and Applications*, vol. 56, no. 3, pp. 507–530, 2013.
- [4] C. A. Metzler, A. Maleki, and R. G. Baraniuk, “From denoising to compressed sensing,” *IEEE Transactions on Information Theory*, vol. 62, no. 9, pp. 5117–5144, 2016.
- [5] K. Kulkarni, S. Lohit, P. Turaga, R. Kerviche, and A. Ashok, “Reconnet: Non-iterative reconstruction of images from compressively sensed measurements,” in *Proceedings of the IEEE Conference on Computer Vision and Pattern Recognition*, 2016, pp. 449–458.
- [6] C. A. Metzler, A. Mousavi, and R. G. Baraniuk, “Learned d-amp: Principled neural network based compressive image recovery,” *arXiv preprint arXiv:1704.06625*, 2017.
- [7] J. Zhang and B. Ghanem, “Ista-net: Interpretable optimization-inspired deep network for image compressive sensing,” in *Proceedings of the IEEE conference on computer vision and pattern recognition*, 2018, pp. 1828–1837.
- [8] K. Xu, Z. Zhang, and F. Ren, “Lapran: A scalable laplacian pyramid reconstructive adversarial network for flexible compressive sensing reconstruction,” in *Proceedings of the European Conference on Computer Vision (ECCV)*, 2018, pp. 485–500.
- [9] A. Bora, A. Jalal, E. Price, and A. G. Dimakis, “Compressed sensing using generative models,” in *International Conference on Machine Learning*. PMLR, 2017, pp. 537–546.
- [10] Y. Wu, M. Rosca, and T. Lillicrap, “Deep compressed sensing,” in *International Conference on Machine Learning*. PMLR, 2019, pp. 6850–6860.
- [11] A. Paszke, S. Gross, F. Massa, A. Lerer, J. Bradbury, G. Chanan, T. Killeen, Z. Lin, N. Gimelshein, L. Antiga *et al.*, “Pytorch: An imperative style, high-performance deep learning library,” *arXiv preprint arXiv:1912.01703*, 2019.
- [12] M. Abadi, P. Barham, J. Chen, Z. Chen, A. Davis, J. Dean, M. Devin, S. Ghemawat, G. Irving, M. Isard *et al.*, “Tensorflow: A system for large-scale machine learning,” in *12th {USENIX} symposium on operating systems design and implementation ({OSDI} 16)*, 2016, pp. 265–283.
- [13] Y. LeCun, L. Bottou, Y. Bengio, and P. Haffner, “Gradient-based learning applied to document recognition,” *Proceedings of the IEEE*, vol. 86, no. 11, pp. 2278–2324, 1998.
- [14] A. Krizhevsky, G. Hinton *et al.*, “Learning multiple layers of features from tiny images,” 2009.
- [15] Z. Liu, P. Luo, X. Wang, and X. Tang, “Deep learning face attributes in the wild,” in *Proceedings of International Conference on Computer Vision (ICCV)*, December 2015.
- [16] J. Kim, J. Kwon Lee, and K. Mu Lee, “Accurate image super-resolution using very deep convolutional networks,” in *Proceedings of the IEEE conference on computer vision and pattern recognition*, 2016, pp. 1646–1654.
- [17] W.-S. Lai, J.-B. Huang, N. Ahuja, and M.-H. Yang, “Deep laplacian pyramid networks for fast and accurate super-resolution,” in *Proceedings of the IEEE conference on computer vision and pattern recognition*, 2017, pp. 624–632.
- [18] S. Schulter, C. Leistner, and H. Bischof, “Fast and accurate image upscaling with super-resolution forests,” in *Proceedings of the IEEE conference on computer vision and pattern recognition*, 2015, pp. 3791–3799.
- [19] J. Yang, J. Wright, T. S. Huang, and Y. Ma, “Image super-resolution via sparse representation,” *IEEE transactions on image processing*, vol. 19, no. 11, pp. 2861–2873, 2010.
- [20] P. Arbelaez, M. Maire, C. Fowlkes, and J. Malik, “Contour detection and hierarchical image segmentation,” *IEEE transactions on pattern analysis and machine intelligence*, vol. 33, no. 5, pp. 898–916, 2010.
- [21] M. Bevilacqua, A. Roumy, C. Guillemot, and M. L. Alberi-Morel, “Low-complexity single-image super-resolution based on nonnegative neighbor embedding,” 2012.
- [22] R. Zeyde, M. Elad, and M. Protter, “On single image scale-up using sparse-representations,” in *International conference on curves and surfaces*. Springer, 2010, pp. 711–730.
- [23] A. Radford, L. Metz, and S. Chintala, “Unsupervised representation learning with deep convolutional generative adversarial networks,” *arXiv preprint arXiv:1511.06434*, 2015.
- [24] T. Karras, S. Laine, and T. Aila, “A style-based generator architecture for generative adversarial networks,” in *Proceedings of the IEEE/CVF Conference on Computer Vision and Pattern Recognition*, 2019, pp. 4401–4410.

V. APPENDIX

Dataset	Compression ratio	PSNR	SSIM	Reconstruction per second
MNIST	2	48	0.9999	4.0112
MNIST	4	47.2738	0.9997	4.0519
MNIST	8	30.4165	0.9704	4.0733
MNIST	16	24.7801	0.9287	5.9312
MNIST	32	14.0546	0.5527	18.8679
CelebA	2	40.5767	0.9986	1.0279
CelebA	4	32.1129	0.9911	1.0635
CelebA	8	27.5632	0.9759	1.0615
CelebA	16	23.7575	0.9409	1.0586
CelebA	32	17.6439	0.7866	5.0302
CIFAR10	2	35.1305	0.995	4.3422
CIFAR10	4	28.6455	0.9793	4.1477
CIFAR10	8	22.7897	0.9323	4.1789
CIFAR10	16	18.395	0.823	6.8776
CIFAR10	32	13.7681	0.4758	51.5464
CIFAR10(Gray)	2	34.5538	0.9945	4.0816
CIFAR10(Gray)	4	28.1537	0.9775	4.0552
CIFAR10(Gray)	8	23.3344	0.938	3.8730
CIFAR10(Gray)	16	17.2754	0.7614	14.4928
CIFAR10(Gray)	32	13.7009	0.4419	27.1003
Bigset	2	37.2695	0.9951	0.9595
Bigset	4	33.8795	0.9879	1.0145
Bigset	8	31.0234	0.9742	1.0199
Bigset	16	28.01	0.9524	1.0109
Bigset	32	17.51	0.7634	4.3821
Bigset(Gray)	2	40.4972	0.9954	0.8445
Bigset(Gray)	4	37.3146	0.9881	0.8602
Bigset(Gray)	8	34.1416	0.975	0.8648
Bigset(Gray)	16	32.9576	0.9651	0.6353
Bigset(Gray)	32	13.5395	0.5392	3.8066

TABLE VI
BENCHMARK RESULTS OF LDAMP

Dataset	Compression ratio	PSNR	SSIM	Reconstruction per second
MNIST	2	47.6	0.9994	93.4579
MNIST	4	41.5	0.9975	55.2486
MNIST	8	32.68	0.9819	75.7576
MNIST	16	23.35	0.8752	75.7576
MNIST	32	14.37	0.5014	82.6446
CelebA	2	37.43	0.9798	11.9190
CelebA	4	31.14	0.9297	14.3062
CelebA	8	27.07	0.8499	4.8170
CelebA	16	23.77	0.7406	7.3475
CelebA	32	21.13	0.6295	17.5439
CIFAR10	2	34.12	0.9703	30.1205
CIFAR10	4	27.66	0.8932	33.2226
CIFAR10	8	23.41	0.7632	31.4465
CIFAR10	16	20.25	0.5979	25.9067
CIFAR10	32	17.95	0.435	26.3852
CIFAR10(Gray)	2	33.63	0.9679	138.8889
CIFAR10(Gray)	4	27.46	0.8886	68.0272
CIFAR10(Gray)	8	23.15	0.7501	75.1880
CIFAR10(Gray)	16	20.25	0.5911	81.3008
CIFAR10(Gray)	32	18.13	0.4406	86.2069
Bigset	2	37.28	0.9393	15.8479
Bigset	4	33	0.8686	19.5313
Bigset	8	29.88	0.7823	22.0751
Bigset	16	27.03	0.682	25.6410
Bigset	32	24.67	0.5864	29.7619
Bigset(Gray)	2	38.49	0.95	57.8035
Bigset(Gray)	4	34.06	0.8874	76.9231
Bigset(Gray)	8	30.69	0.8007	82.6446
Bigset(Gray)	16	27.66	0.7035	74.0741
Bigset(Gray)	32	25.16	0.6074	65.3595

TABLE VII
BENCHMARK RESULTS OF ISTA-NET

Dataset	Compression ratio	PSNR	SSIM	Reconstruction per second
MNIST	2	29.21261238	0.963992	128.4409
MNIST	4	30.511987	0.9563419	125.7462
MNIST	8	29.1593111	0.95584067	123.5473
MNIST	16	25.24258976	0.9275	126.5051
MNIST	32	21.34934368	0.8455416	121.4136
CelebA	2	20.2155866	0.81079007	3.9383
CelebA	4	17.71371	0.68814778	4.3050
CelebA	8	18.014066	0.7477318	4.6045
CelebA	16	21.0597539	0.84389696	4.6687
CelebA	32	21.5447282	0.85383977	4.6963
CIFAR10	2	19.83498	0.8109526	6.1278
CIFAR10	4	21.60267	0.864623124	6.1788
CIFAR10	8	21.78964748	0.869176	6.1605
CIFAR10	16	21.22622989	0.85057847	6.1618
CIFAR10	32	19.76376	0.79459368	6.1814
CIFAR10(Gray)	2	23.4110478	0.75807036	6.2749
CIFAR10(Gray)	4	22.850186	0.7317556	6.2010
CIFAR10(Gray)	8	21.788798	0.679377	6.2342
CIFAR10(Gray)	16	19.729784	0.5493096	6.2563
CIFAR10(Gray)	32	18.11486	0.428783	6.2666
Bigset	2	18.1686235	0.53700839	3.8009
Bigset	4	16.37976747	0.387361	4.1351
Bigset	8	17.64976	0.4810631	4.3130
Bigset	16	21.48601	0.63840458	4.4691
Bigset	32	21.016629	0.63255624	4.4737
Bigset(Gray)	2	18.22068	0.2186767	4.4920
Bigset(Gray)	4	21.52289	0.387422	4.5158
Bigset(Gray)	8	23.2502995	0.537785	4.5220
Bigset(Gray)	16	23.5321	0.54008	4.4926
Bigset(Gray)	32	22.8348	0.508885	4.4470

TABLE VIII
BENCHMARK RESULTS OF CSGAN

Dataset	Compression ratio	PSNR	SSIM	Reconstruction per second
MNIST	2	32.0483	0.9156	223.1187
MNIST	4	32.1388	0.9869	221.9279
MNIST	8	26.5582	0.954	222.8450
MNIST	16	23.3674	0.8691	229.3073
MNIST	32	19.7423	0.7701	219.0102
CelebA	2	29.4438	0.975	137.9121
CelebA	4	33.2433	0.9888	150.3084
CelebA	8	28.9183	0.9698	146.9329
CelebA	16	26.2793	0.9483	151.5757
CelebA	32	23.1517	0.8969	151.6358
CIFAR10	2	31.6029	0.9862	174.7553
CIFAR10	4	27.808	0.9674	225.8276
CIFAR10	8	25.4534	0.9428	227.8823
CIFAR10	16	22.262	0.8844	230.9234
CIFAR10	32	19.852	0.7874	214.7841
CIFAR10(Gray)	2	25.7358	0.8669	141.5323
CIFAR10(Gray)	4	23.6409	0.7804	219.8296
CIFAR10(Gray)	8	21.621	0.6675	229.1173
CIFAR10(Gray)	16	19.6054	0.5293	223.8697
CIFAR10(Gray)	32	18.0317	0.3887	232.5259
Bigset	2	30.7518	0.9314	30.5301
Bigset	4	30.2502	0.9214	34.1619
Bigset	8	28.3798	0.881	36.4556
Bigset	16	27.3575	0.8539	34.5518
Bigset	32	24.035	0.7489	41.8374
Bigset(Gray)	2	30.5937	0.8376	35.3011
Bigset(Gray)	4	30.2819	0.8125	41.4439
Bigset(Gray)	8	27.0031	0.7037	32.2543
Bigset(Gray)	16	25.1241	0.6216	41.1410
Bigset(Gray)	32	23.6821	0.5611	44.2111

TABLE IX
BENCHMARK RESULTS OF LAPRAN

Dataset	Compression ratio	PSNR	SSIM	Reconstruction per second
MNIST	2	22.8994	0.9097095	0.0203
MNIST	4	22.8033897	0.907734	0.0239
MNIST	8	22.606246	0.90343	0.0262
MNIST	16	22.122029	0.8913968	0.0269
MNIST	32	20.711256	0.84612	0.0288
CelebA	2	21.045856	0.6081025	0.0003
CelebA	4	20.93657	0.60344236	0.0006
CelebA	8	20.71776	0.593764	0.0007
CelebA	16	20.265672	0.57368156	0.0010
CelebA	32	19.326236	0.5305725	0.0026
CIFAR10	2	19.3796396	0.5837099	0.0048
CIFAR10	4	19.09479988	0.567872	0.0062
CIFAR10	8	18.5491	0.5368614	0.0070
CIFAR10	16	17.4882184	0.47517336	0.0076
CIFAR10	32	15.74646	0.375408	0.0078
CIFAR10(Gray)	2	18.87746	0.562994	0.0077
CIFAR10(Gray)	4	18.11757	0.519013	0.0079
CIFAR10(Gray)	8	16.7601456	0.44195844	0.0080
CIFAR10(Gray)	16	14.702925	0.3263529	0.0081
CIFAR10(Gray)	32	12.44196	0.20419125	0.0081
Bigset	2	20.585639	0.4295568	0.0005
Bigset	4	20.52696	0.427472	0.0009
Bigset	8	20.38664	0.4207375	0.0012
Bigset	16	20.09884	0.4053666	0.0016
Bigset	32	19.56	0.3787025	0.0024
Bigset(Gray)	2	20.51396	0.44394666	0.0017
Bigset(Gray)	4	20.23436	0.4295096	0.0026
Bigset(Gray)	8	19.72645	0.402825	0.0036
Bigset(Gray)	16	18.6832379	0.35273	0.0040
Bigset(Gray)	32	16.828574	0.271182335	0.0042

TABLE X
BENCHMARK RESULTS OF CSGM

Dataset	Compression ratio	PSNR	SSIM	Reconstruction per second
MNIST	2	32.260701	0.972028	322.6847
MNIST	4	29.205807	0.94958	337.0408
MNIST	8	26.095692	0.934991	340.7155
MNIST	16	22.985161	0.858342	330.0330
MNIST	32	19.731156	0.759906	308.5467
CelebA	2	31.146907	0.928824	197.1998
CelebA	4	28.221271	0.879022	185.2195
CelebA	8	25.431465	0.807207	187.4063
CelebA	16	23.088657	0.719763	203.8320
CelebA	32	21.078599	0.634741	212.3593
CIFAR10	2	28.837922	0.925328	242.3655
CIFAR10	4	25.025284	0.83476	242.0721
CIFAR10	8	21.818953	0.695573	252.3978
CIFAR10	16	19.687775	0.556359	253.9360
CIFAR10	32	17.884739	0.419771	270.8559
CIFAR10(Gray)	2	28.976893	0.926141	356.6334
CIFAR10(Gray)	4	25.305743	0.838226	382.8484
CIFAR10(Gray)	8	22.079408	0.69848	378.2148
CIFAR10(Gray)	16	19.853126	0.555715	381.2429
CIFAR10(Gray)	32	18.131324	0.417519	341.0641
Bigset	2	31.407366	0.861091	176.1804
Bigset	4	28.871363	0.78055	211.7747
Bigset	8	26.969953	0.703401	212.4947
Bigset	16	24.779469	0.61489	183.3853
Bigset	32	23.04078	0.538448	215.4708
Bigset(Gray)	2	32.843938	0.88696	264.8305
Bigset(Gray)	4	30.512706	0.822898	305.4368
Bigset(Gray)	8	27.992924	0.73558	312.4024
Bigset(Gray)	16	26.045158	0.656687	294.8983
Bigset(Gray)	32	23.929067	0.566278	300.4808

TABLE XI
BENCHMARK RESULTS OF RECONNET

Dataset	Compression ratio	PSNR	SSIM	Reconstruction per second
MNIST	2	47.995	1	16.3934
MNIST	4	33.233	0.879	12.3457
MNIST	8	20.587	0.542	12.3457
MNIST	16	15.291	0.299	15.8730
MNIST	32	13.076	0.163	16.1290
CelebA	2	32.335	0.959	0.7283
CelebA	4	26.592	0.889	1.2516
CelebA	8	22.863	0.801	1.2563
CelebA	16	19.919	0.703	1.4104
CelebA	32	17.345	0.599	1.4025
CIFAR10	2	29.584	0.936	4.6948
CIFAR10	4	24.001	0.822	4.6083
CIFAR10	8	20.621	0.69	4.8077
CIFAR10	16	18.286	0.573	5.2356
CIFAR10	32	16.401	0.476	5.3476
CIFAR10(Gray)	2	29.766	0.9	14.4928
CIFAR10(Gray)	4	24.189	0.742	13.1579
CIFAR10(Gray)	8	20.778	0.577	13.6986
CIFAR10(Gray)	16	18.343	0.446	15.3846
CIFAR10(Gray)	32	16.661	0.362	16.1290
Bigset	2	35.83	0.96	0.7962
Bigset	4	31.084	0.905	1.3106
Bigset	8	27.632	0.845	1.3298
Bigset	16	24.754	0.786	1.4286
Bigset	32	22.109	0.729	1.4225
Bigset(Gray)	2	36.154	0.915	1.6447
Bigset(Gray)	4	31.368	0.814	3.5971
Bigset(Gray)	8	27.871	0.711	3.9063
Bigset(Gray)	16	24.954	0.62	4.2735
Bigset(Gray)	32	22.054	0.545	4.0984

TABLE XII
BENCHMARK RESULTS OF TVAL-3

Dataset	Compression ratio	PSNR	SSIM	Reconstruction per second
MNIST	2	47.911	0.999	0.8569
MNIST	4	31.01	0.803	0.8244
MNIST	8	19.881	0.489	0.8244
MNIST	16	14.158	0.225	1.0132
MNIST	32	11.762	0.1	1.1779
CelebA	2	32.578	0.961	0.0307
CelebA	4	27.003	0.897	0.0487
CelebA	8	23.359	0.816	0.0516
CelebA	16	20.721	0.731	0.0531
CelebA	32	18.235	0.633	0.0471
CIFAR10	2	30.078	0.943	0.2993
CIFAR10	4	24.486	0.837	0.3171
CIFAR10	8	21.115	0.709	0.2793
CIFAR10	16	18.697	0.584	0.3167
CIFAR10	32	16.746	0.476	0.3738
CIFAR10(Gray)	2	30.231	0.91	0.7868
CIFAR10(Gray)	4	24.619	0.758	1.0030
CIFAR10(Gray)	8	21.328	0.596	0.9891
CIFAR10(Gray)	16	18.822	0.452	1.0194
CIFAR10(Gray)	32	17.046	0.344	1.1173
Bigset	2	36.084	0.961	0.0351
Bigset	4	31.6	0.91	0.0522
Bigset	8	28.475	0.855	0.0554
Bigset	16	25.951	0.802	0.0568
Bigset	32	23.821	0.754	0.0599
Bigset(Gray)	2	36.425	0.919	0.0862
Bigset(Gray)	4	31.881	0.823	0.1557
Bigset(Gray)	8	28.687	0.727	0.1642
Bigset(Gray)	16	26.128	0.64	0.1740
Bigset(Gray)	32	24.035	0.57	0.1671

TABLE XIII
BENCHMARK RESULTS OF L1

Dataset	Compression ratio	PSNR	SSIM	Reconstruction per second
MNIST	2	43.45	0.972	0.3483
MNIST	4	31.787	0.891	0.3526
MNIST	8	22.582	0.724	0.3407
MNIST	16	13.238	0.322	0.3274
MNIST	32	6.53	0.093	0.3194
CelebA	2	47.126	0.998	0.0568
CelebA	4	37.495	0.985	0.0537
CelebA	8	31.095	0.95	0.0458
CelebA	16	26.328	0.877	0.0450
CelebA	32	21.517	0.723	0.0500
CIFAR10	2	40.401	0.993	0.2190
CIFAR10	4	31.595	0.957	0.2104
CIFAR10	8	25.851	0.867	0.1976
CIFAR10	16	20.248	0.645	0.1882
CIFAR10	32	8.307	0.113	0.1843
CIFAR10(Gray)	2	31.682	0.929	0.3606
CIFAR10(Gray)	4	25.616	0.789	0.3524
CIFAR10(Gray)	8	19.996	0.537	0.3398
CIFAR10(Gray)	16	16.365	0.342	0.3418
CIFAR10(Gray)	32	8.016	0.074	0.3398
Bigset	2	42.51	0.992	0.0474
Bigset	4	37.565	0.977	0.0520
Bigset	8	33.95	0.949	0.0516
Bigset	16	30.973	0.908	0.0480
Bigset	32	27.3	0.832	0.0496
Bigset(Gray)	2	38.205	0.94	0.1224
Bigset(Gray)	4	34.138	0.87	0.1222
Bigset(Gray)	8	30.774	0.786	0.1216
Bigset(Gray)	16	27.234	0.67	0.1221
Bigset(Gray)	32	20.727	0.435	0.1216

TABLE XIV
BENCHMARK RESULTS OF D-AMP

Dataset	Compression ratio	PSNR	SSIM	Reconstruction per second
MNIST	2	40.062	0.912	0.3148
MNIST	4	29.452	0.778	0.3264
MNIST	8	18.787	0.472	0.3270
MNIST	16	15.058	0.312	0.3247
MNIST	32	12.052	0.132	0.3258
CelebA	2	35.932	0.978	0.0238
CelebA	4	29.288	0.93	0.0233
CelebA	8	23.97	0.831	0.0231
CelebA	16	21.211	0.743	0.0233
CelebA	32	17.848	0.601	0.0232
CIFAR10	2	30.627	0.938	0.1019
CIFAR10	4	24.975	0.843	0.1055
CIFAR10	8	21.008	0.7	0.1055
CIFAR10	16	18.564	0.576	0.1063
CIFAR10	32	16.928	0.477	0.1073
CIFAR10(Gray)	2	31.14	0.912	0.3108
CIFAR10(Gray)	4	25.336	0.781	0.3312
CIFAR10(Gray)	8	21.215	0.598	0.3295
CIFAR10(Gray)	16	18.81	0.463	0.3301
CIFAR10(Gray)	32	16.921	0.353	0.3318
Bigset	2	38.114	0.973	0.0240
Bigset	4	33.706	0.938	0.0243
Bigset	8	30.003	0.883	0.0244
Bigset	16	27.201	0.831	0.0249
Bigset	32	24.191	0.758	0.0249
Bigset(Gray)	2	38.697	0.942	0.0720
Bigset(Gray)	4	34.293	0.874	0.0728
Bigset(Gray)	8	30.449	0.781	0.0726
Bigset(Gray)	16	27.393	0.692	0.0741
Bigset(Gray)	32	24.426	0.592	0.0744

TABLE XV
BENCHMARK RESULTS OF NLR-CS